Band gap tunability of magneto-elastic phononic crystal

Olivier Bou Matar, J.F. Robillard, Jerome O. Vasseur, Anne-Christine Hladky, P.A. Deymier, Philippe Pernod, Vladimir Preobrazhensky

Band gap tunability of magneto-elastic phononic crystal

Cite as: J. Appl. Phys. **111**, 054901 (2012); https://doi.org/10.1063/1.3687928
Submitted: 18 November 2011 • Accepted: 28 January 2012 • Published Online: 01 March 2012

O. Bou Matar, J. F. Robillard, J. O. Vasseur, et al.

Band gap tunability of magneto-elastic phononic crystal

O. Bou Matar,[1,a)] J. F. Robillard,[2] J. O. Vasseur,[2] A.-C. Hladky-Hennion,[2] P. A. Deymier,[3] P. Pernod,[1] and V. Preobrazhensky[4]
[1]*International Associated Laboratory LEMAC: IEMN, UMR CNRS 8520, PRES Lille Nord de France, ECLille, 59652 Villeneuve d'Ascq, France*
[2]*Institut d'Electronique, Microelectronique et Nanotechnologie (IEMN, UMR CNRS 8520), PRES Lille Nord de France, 59652 Villeneuve d'Ascq, France*
[3]*Department of Materials Science and Engineering, University of Arizona, Tucson, Arizona 85721, USA*
[4]*International Associated Laboratory LEMAC: Wave Research Center, GPI RAS, 38 Vavilov str., Moscow, 119991, Russia*

(Received 18 November 2011; accepted 28 January 2012; published online 1 March 2012)

The possibility of control and tuning of the band structures of phononic crystals offered by the introduction of an active magnetoelastic material and the application of an external magnetic field is studied. Two means to obtain large elastic properties variations in magnetoelastic material are considered: Giant magnetostriction and spin reorientation transition effects. A plane wave expansion method is used to calculate the band structures. The magnetoelastic coupling is taken into account through the consideration of an equivalent piezomagnetic material model with elastic, piezomagnetic, and magnetic permeability tensors varying as a function of the amplitude and orientation of the applied magnetic field. Results of contactless tunability of the absolute bandgap are presented for a two-dimensional phononic crystal constituted of Terfenol-D square rod embedded in an epoxy matrix. © *2012 American Institute of Physics*. [http://dx.doi.org/10.1063/1.3687928]

I. INTRODUCTION

The concept of phononic crystals emerged in the early 1990s as an extension of work done on photonic crystal, *i.e.*, artificial structures whose dielectric permittivity and magnetic permeability are both periodic functions of the position. Phononic crystals are the elastic counterparts to photonic crystals and consist of periodic arrangements of inclusions in a physically dissimilar matrix.[1,2] Due to their periodic structure and under certain conditions of geometry and composition, phononic crystals may exhibit absolute band gaps where the propagation of elastic wave is forbidden independently of the direction of propagation. The existence of forbidden bands confers to phononic crystals numerous potential applications. For instance, in the frequency range of the forbidden band, a phononic crystal behaves as a perfect mirror and an incident wave is perfectly reflected outside of the artificial structure. Phononic crystals may be used as efficient sonic insulators. Some authors have also shown that the removal of inclusions along some pathway in the phononic crystal, produces acoustic waveguides.[3–6] Acoustic waves that would not propagate otherwise in a phononic crystal can be guided with minimal loss along such waveguides. Low loss transmission can be achieved in linear wave guides as well as guides with sharp bends. That opens possibilities for the design of devices allowing the filtering or the demultiplexing of acoustic waves at the scale of the wavelength.[7,8] More specifically it has been shown numerically and experimentally that such structures manufactured at the micrometer scale behave as high Q micromechanical resonators with high resonance frequencies and can be integrated in devices for wireless communications and sensing applications.[9–12] Moreover some dispersion curves in the band structure of a phononic crystal may present a negative curvature, *i.e.*, the Poynting vector and the wave vector, associated to energy flux and phase velocity are opposite in sign. This property may lead to the negative refraction of acoustic waves for frequencies falling in the frequency domain of the band with negative curvature.[13,14] Negative refraction allows for the focusing of acoustic waves with a resolution lower than the diffraction limit[15,16] as well as for the autocollimation of an acoustic beam.[17,18]

Phononic crystal may have applications to numerous technological fields. Nevertheless, for enhanced functionality it appears necessary to introduce a certain degree of frequency tunability of phononic crystals properties. Different answers to this problem have been proposed by several authors. Tunability could be achieved by changing the geometry of the inclusions[19] or by varying the elastic characteristics of the constitutive materials through application of external stimuli.[20] For instance, some authors have proposed the use of electrorheological materials in conjunction with application of external electric field.[21] Other authors have considered the effect of temperature on the elastic moduli.[22,23] In all cases, significant effect on the band structure of the phononic crystal can only be achieved by applying stimuli with very large magnitude. Other authors[24] exploit the change of the structure of the phononic crystal due to an external stress to alter the band structure. However this approach requires physical contact with the phononic crystal. A last proposed solution requires using active materials as constituents of the composite material. Following this way, some authors[25] have studied how the piezoelectric effect can influence the elastic properties of the system and therefore can change the dispersion curves and in particular the gaps.

[a)]Electronic mail: olivier.boumatar@iemn.univ-lille1.fr.

For an arrangement of piezoelectric cylinders embedded in a polymer matrix, they show that the effect is significant for large filling fractions but negligibly small for small ones.[26] Several studies have reported noticeable changes in the band structures of magnetoelectroelastic phononic crystals when the coupling between magnetic, electric, and elastic phenomena are taken into account.[27,28] These studies however do not consider the effect of an external magnetic field on the properties of the phononic crystal. In a recent paper, we demonstrated that the band structure of a two-dimensional phononic crystal constituted of a square array of Terfenol-D square rods embedded in an epoxy resin matrix[29] can be controlled by application of an external magnetic field. Indeed, the elastic properties of magnetoelastic material are very sensitive to its magnetic state and on the applied magnetic field. For instance, in giant magnetostrictive material, such as Terfenol-D, this dependence can lead to more than 50% variation of some of the elastic constants, even at ultrasonic frequencies.[30] So, if one of the components of a phononic crystal is a magneto-elastic medium, then one can expect that the elastic contrast, and subsequently the crystal properties, *e.g.*, the bang gaps frequencies and widths, the negative refraction behaviors, could be controlled without any contact by a magnetic field.

In the present paper, we give a complete derivation of the model presented succinctly in our previous letter,[29] and use it to study in details the tuning of the properties of a bulk magnetoelastic phononic crystal, with both square and triangular lattices, when an external magnetic field is applied. Moreover, we introduce here a new way to obtain huge tuning of the band structures of a magneto-elastic phononic crystal. Indeed, contrary to previous works,[29,31] we consider two-dimensional magneto-elastic phononic crystals in which the tuning can be induced not only by giant magnetostriction, but also by spin-reorientation phase transitions.[32,33]

To be able to consider arbitrary direction and amplitude of the applied magnetic field, we will first derive an equivalent piezomagnetic material of a polarized ferromagnet, with field dependent elastic C_{ijkl}, piezomagnetic q_{lij} and magnetic permeability μ_{ij} constants. This is an extension of the effective elastic moduli method classically used to describe elastic dynamics of a homogeneous magneto-elastic medium.[32,34] But this latter method leads to a dependence of the obtained effective elastic moduli on the propagation direction when the magnetic dipole interaction is taken into account.[35,36] This dependence makes these effective elastic moduli unsuitable for standard numerical tools developed for the calculation of phononic crystal characteristics (band structures, equifrequency curves, transmission, and reflection coefficients …), such as plane wave expansion (PWE) or finite element method (FEM), in the case of a magneto-elastic phononic crystal. On the contrary, as will be shown in Sec. II, the equivalent piezomagnetic material formulation, leading to equations similar to the ones classically used for piezoelectric materials, enables the direct use of PWE and FEM methods developed for the calculation of phononic crystal characteristics in piezoelectric media.[25,37,38] In Sec. III, calculation of the effective piezomagnetic material properties for a varying external magnetic field amplitude and direction, and its implication in the tuning of the band structure of a phononic crystal constituted of a square array of Terfenol-D square rods embedded in an epoxy matrix will be presented and discussed.

II. PIEZOMAGNETIC EQUIVALENT MATERIAL FORMULATION

A. Formulation of the problem: Basic equations

We consider here a magneto-elastic wave in a ferromagnet magnetized to saturation. In this case, the amplitude of the magnetization per unit mass $\boldsymbol{\mu}$ is a constant μ_s. The coupled equations for the mechanical and magnetic systems, *i.e.*, the equation of motion and the Landau-Lifshitz equation, have in the Lagrangian coordinates a_i the form[36,40,41]

$$\rho_0 \frac{\partial^2 u_i}{\partial t^2} = \frac{\partial P_{ij}}{\partial a_j} + \rho_0 \mu_n \frac{\partial H_n}{\partial a_j} \frac{\partial a_j}{\partial x_i}, \tag{1}$$

$$\frac{\partial \boldsymbol{\mu}}{\partial t} = -\gamma \boldsymbol{\mu}_0 \boldsymbol{\mu} \times \boldsymbol{H}_{\text{eff}}, \tag{2}$$

where γ is the gyromagnetic ratio, ρ_0 is the mass density before deformation, μ_0 is the permeability of vacuum, u_i is the ith component of the particle displacement, and x_i denotes the Eulerian coordinates. The magnetization per unit volume is given by $\boldsymbol{M} = \rho \boldsymbol{\mu}$, where ρ is the mass density after deformation. The magnetic-body force term, *i.e.*, the second term in the right hand side of Eq. (1), is due to the interaction of the magnetization with non uniform magnetic fields. The effective internal magnetic field $\boldsymbol{H}_{eff}$ and the Piola-Kirchoff stress tensor P_{ij} are given by

$$H_{eff\,i} = H_i - \frac{1}{\mu_0 \rho_0} \frac{\partial U}{\partial \mu_i} + \frac{1}{\mu_0 \rho_0} \frac{\partial}{\partial a_s} \frac{\partial U}{\partial (\partial \mu_i / \partial a_s)} \tag{3}$$

and

$$P_{ij} = \frac{\partial U}{\partial \eta_{pj}} \frac{\partial x_i}{\partial a_p}, \tag{4}$$

where $\boldsymbol{H}$ is the Maxwellian magnetic field, and η_{kl} is the strain tensor

$$\eta_{ij} = \frac{1}{2} \left(\frac{\partial u_i}{\partial a_j} + \frac{\partial u_j}{\partial a_i} + \frac{\partial u_k}{\partial a_i} \frac{\partial u_k}{\partial a_j} \right). \tag{5}$$

Here, U is the local internal energy per unit volume that can be written in the following form:

$$U = U_{an} + U_{me} + U_e, \tag{6}$$

where the magnetocrystalline anisotropy, magneto-elastic coupling, and elastic energies, are respectively, given by

$$U_{an} = K_{ij} \alpha_i \alpha_j + K_{ijkl} \alpha_i \alpha_j \alpha_k \alpha_l, \tag{7}$$

$$U_{me} = b_{ijkl} \alpha_i \alpha_j \eta_{kl}, \tag{8}$$

$$U_e = \frac{1}{2} C_{ijkl} \eta_{ij} \eta_{kl}. \tag{9}$$

$\alpha_i = \mu_i/\mu_s$ are the direction cosines of $\boldsymbol{\mu}$ (or $\boldsymbol{M}$) with respect to the symmetry axes, K_{ij} and K_{ijkl} are the magnetic anisotropy constants, b_{ijkl} are the magneto-elastic constants, and C_{ijkl} are the second-order elastic constants. Here, in the considered acoustic frequency range (up to a few GHz), the elastic wavelengths are much greater than the atomic spacing so that exchange effects may be neglected. In the case of a cubic ferromagnet, such as the Terfenol-D considered in the numerical example, the local internal energy density can be, in the crystallographic axis, written as

$$\begin{aligned} U = {} & K_1\left(\alpha_1^2\alpha_2^2 + \alpha_1^2\alpha_3^2 + \alpha_2^2\alpha_3^2\right) + B_1\left(\eta_{11}\alpha_1^2 + \eta_{22}\alpha_2^2 + \eta_{33}\alpha_3^2\right) \\ & + B_2(\eta_{12}\alpha_1\alpha_2 + \eta_{13}\alpha_1\alpha_3 + \eta_{23}\alpha_2\alpha_3) \\ & + \frac{C_{11}}{2}\left(\eta_{11}^2 + \eta_{22}^2 + \eta_{33}^2\right) + C_{12}(\eta_{11}\eta_{22} + \eta_{11}\eta_{33} + \eta_{22}\eta_{33}) \\ & + 2C_{44}\left(\eta_{12}^2 + \eta_{13}^2 + \eta_{23}^2\right), \end{aligned} \tag{10}$$

where $K_1 = K_{1111}$ is the magnetic anisotropy constant, and $B_1 = b_{1111}$ and $B_2 = 4b_{1212}$ are the magneto-elastic constants.

As we are interested in acoustic wave propagation, we consider only small dynamic perturbations around an equilibrium state

$$\boldsymbol{H} = \boldsymbol{H}_0 + \boldsymbol{h},\ \boldsymbol{M} = \boldsymbol{M}_0 + \boldsymbol{m},\ \text{and}\ \boldsymbol{u} = \boldsymbol{u}_0 + \tilde{\boldsymbol{u}}, \tag{11}$$

$\boldsymbol{H}_0$ is the internal field, *i.e.*, the sum of the external applied field and a demagnetizing field, $\boldsymbol{u}_0$ is a spontaneous displacement caused by magnetostriction, and $\boldsymbol{h}$, $\boldsymbol{m}$, and $\tilde{\boldsymbol{u}}$ are the magnetostatic field, magnetization, and displacement generated by the magneto-elastic waves, respectively. Here, as the wavelengths of the magneto-elastic waves are much smaller than the free-space electromagnetic wavelengths, $\boldsymbol{h}$ verifies the magnetostatic equations

$$\nabla \times \boldsymbol{h} = 0 \ \text{and}\ \nabla \cdot \boldsymbol{b} = \nabla \cdot \mu_0\left(\boldsymbol{h} + \frac{\rho}{\rho_0}\boldsymbol{m}\right) = 0, \tag{12}$$

where $\boldsymbol{b}$ is the dynamic magnetic induction and $\rho \approx \rho_0(1 - \eta_{ii})$, where i = 1, 2, or 3. Moreover, while this quasi-static approximation is not strictly true for conducting materials, one can expect it to hold when their dimensions are much smaller than the skin depth. In the considered frequency range, up to a few MHz, this will always be true for all the studied phononic crystal structures.

As we are only interested by field dependent variations of the elastic and piezomagnetic properties of the ferromagnet, arising from the first order magnetoelastic coupling, *i.e.*, the "Simon effect",[42] we neglect all the field independent morphic contributions coming from the magnetoelastic second order coupling and anharmonic terms arising from the second and third order elastic energies.[41,43] Here, the contributions introduced by the rotationally invariant theory of magnetoelastic media[33,44] are also neglected. Indeed, they are negligible in the considered materials, as it will be shown in Sec. IV. In the present paper, as it is always the case in the literature, explicit expressions for the Simon effect are derived assuming that a magnetic field sufficient for eliminating the domain walls has been applied.

B. Equilibrium state

First, the equilibrium values $\boldsymbol{M}_0$ and $\boldsymbol{u}_0$ are found by minimizing the total energy of the magneto-elastic system $U_T = U - \mu_0 \boldsymbol{M}.\boldsymbol{H}$. We assume that the acoustic wave propagation only induces small dynamic perturbations

$$\boldsymbol{m} \ll \boldsymbol{M}_0,\ \boldsymbol{h} \ll \boldsymbol{H}_0 \ \text{ and } \ \tilde{\boldsymbol{u}} \ll \boldsymbol{u}_0. \tag{13}$$

Introducing Eq. (11) into Eq. (2), and allowing for conditions (13), the successive approximations method can be used. In the zero approximation, retaining only static terms, we obtain

$$\boldsymbol{M}_0 \times \boldsymbol{H}_{eff0} = 0. \tag{14}$$

This expression indicates that the equilibrium direction of magnetization $\boldsymbol{M}_0$ is given by the static effective internal magnetic field $\boldsymbol{H}_{eff0}$.

To consider an external static magnetic field $\boldsymbol{H}_{ext}$ in any directions, we use the method of spherical coordinates proposed by Smit and Beljers[45] and Suhl[46] for the study of ferromagnetic resonance in anisotropic media. As the considered ferromagnet is magnetized to saturation, two variables, θ and φ as shown on Fig. 1 are sufficient in place of the three M_i components. In the spherical coordinates the components of the total energy of the magneto-elastic system $U_T = U + U_Z + U_D$, where U is given by Eq. (6), are

$$\begin{aligned} U_Z &= -\mu_0 \boldsymbol{M}.\boldsymbol{H}_{ext} \\ &= -\mu_0 M_s(H_x \sin\theta\cos\varphi + H_y \sin\theta\sin\varphi + \mathrm{H}_z\cos\theta), \end{aligned} \tag{15}$$

$$U_D = -\frac{\mu_0}{2}\boldsymbol{M}.\boldsymbol{H}_D = \frac{\mu_0}{2}\boldsymbol{M}.(\boldsymbol{N}.\boldsymbol{M}), \tag{16}$$

$$U_{an} = \frac{K_1}{4}(\sin^4\theta\sin^2 2\varphi + \sin^2 2\theta), \tag{17}$$

$$\begin{aligned} U_{me} = {} & B_1(\eta_{11}\sin^2\theta\cos^2\varphi + \eta_{22}\sin^2\theta\sin^2\varphi + \eta_{33}\cos^2\theta) \\ & + B_2(\eta_{12}\sin^2\theta\cos\varphi\sin\varphi + \eta_{13}\sin\theta\cos\theta\cos\varphi \\ & + \eta_{23}\sin\theta\cos\theta\sin\varphi). \end{aligned} \tag{18}$$

Here, $M_s = \rho_0\mu_s$, U_Z and U_D are the Zeeman and demagnetizing energies, respectively, and $\boldsymbol{H}_D = -\boldsymbol{N}.\boldsymbol{M}$, where $\boldsymbol{N}$ is

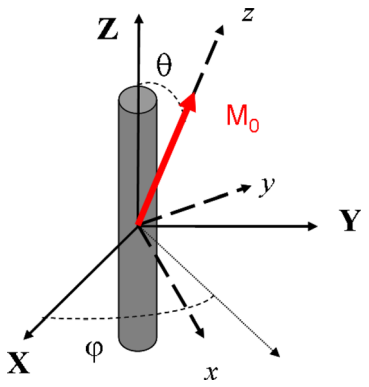

FIG. 1. (Color online) Schematic illustration showing the spherical coordinates used in the calculation. oriented along the Z axis, the demagnetizing tensor is given by Ref. 40.

the demagnetizing tensor. In the case of a rod of infinite length, oriented along the Z axis, the demagnetizing tensor is given by

$$\boldsymbol{N} = \begin{bmatrix} 1/2 & 0 & 0 \\ 0 & 1/2 & 0 \\ 0 & 0 & 0 \end{bmatrix}, \tag{19}$$

leading to $U_D = \mu_0 M_s^2 \sin^2\theta/4$.

The first step, to find the equilibrium state, is to minimize the energy U_T with respect to the strains: $\partial U_T/\partial \eta_{ij} = \partial(U_{me} + U_e)/\partial \eta_{ij}$. The solutions of these six equations, in the case of a crystal with cubic symmetry are given in Appendix A. It can be seen that the existence of a magnetoelastic coupling induces in the sample a uniform static strain. Introducing, now, these expressions of the equilibrium strains in the elastic and magneto-elastic parts of the internal energy, one can write the energy U in the same form as a magneto-crystalline anisotropy energy[47]

$$U = \frac{K_1^*}{4}(\sin^4\theta \sin^2 2\varphi + \sin^2 2\theta), \tag{20}$$

where

$$K_1^* = K_1 + \frac{B_1^2}{C_{11} - C_{12}} - \frac{B_2^2}{8C_{44}}, \tag{21}$$

K_1* is an effective magnetic anisotropy constant taking into account static elastic and magnetoelastic effects. Hence, as the total energy of the magneto-elastic system depends only on the orientation of the magnetization, minimizing the energy with respect to this orientation gives the equilibrium direction (θ_0, φ_0) of $\boldsymbol{M}$, for a given applied field. Knowing this equilibrium position, one can now study the dynamic response of the system to an acoustic perturbation.

C. Piezomagnetic equivalent material

Here, we choose to derive the equivalent piezomagnetic material of the polarized ferromagnet around the equilibrium position. This will allow us to directly use the theoretical and numerical tools, *e.g.*, PWE and FEM methods, developed for the study of piezoelectric or piezomagnetic phononic crystals. A similar approach has been adopted by Ganguly *et al.*[48,49] for the study of the influence of an external magnetic field on the propagation of Rayleigh and Lamb waves in a thin magnetoelastic film deposed on a substrate. But, in this work an equivalent piezomagnetic material has been obtained only in specific configurations.

First, the Landau-Lifshitz equations are rewritten in the used spherical coordinates

$$\begin{aligned} \frac{\partial\theta}{\partial t} &= -\frac{\gamma}{M_s \sin\theta}\frac{\partial U}{\partial \varphi} + \gamma\mu_0 H^{\varphi} = \gamma\mu_0 H_{eff}^{\varphi} \\ \frac{\partial\varphi}{\partial t} &= \frac{\gamma}{M_s \sin\theta}\frac{\partial U}{\partial \theta} - \frac{\gamma}{\sin\theta}\mu_0 H^{\theta} = -\frac{\gamma}{\sin\theta}\mu_0 H_{eff}^{\theta}, \end{aligned} \tag{22}$$

where $H^{\varphi} = -H_x \sin\varphi + \mathrm{H}_y \cos\varphi$, and $H^{\theta} = H_x \cos\theta\cos\varphi + \mathrm{H}_y \cos\theta\sin\varphi - H_z \sin\theta$. The acoustic perturbation rotates the magnetization to a new θ and φ orientation, where $\theta = \theta_0 + \delta\theta$ and $\varphi = \varphi_0 + \delta\varphi$, with $\delta\theta,\ \delta\varphi \gg 1$. Then, the energy is expended around the equilibrium position:

$$\begin{aligned} U = U_0 &+ U_\theta \delta\theta + U_\varphi \delta\varphi + U_{\theta\theta}/2\delta\theta^2 + U_{\varphi\varphi}/2\delta\varphi^2 \\ &+ U_{\theta\varphi}\delta\theta\delta\varphi + U_{\theta\varepsilon_{ij}}\delta\theta\partial u_i/\partial a_j + U_{\varphi\varepsilon_{ij}}\delta\varphi\partial u_i/\partial a_j, \end{aligned} \tag{23}$$

where U_x and U_{xy} denote the first and second order x or x-y derivative of U, respectively.

In the frequency range of elastic wave, $\omega \ll \omega_S$ where ω_S is the natural frequency of spin mode, the magnetic subsystem has time to adjust itself to the elastic subsystem, leading to the following conditions $\partial U_T/\partial(\delta\theta) = 0$ and $\partial U_T/\partial(\delta\varphi) = 0$. These conditions enable us to write $\delta\theta$ and $\delta\varphi$, as functions of $\tilde{\boldsymbol{u}}$ and $\boldsymbol{h}$:

$$\begin{aligned} \delta\theta &= \frac{\mu_0}{D} M_s U'_{\varphi\varphi} h^{\theta} - \frac{\mu_0}{D} M_s \sin\theta_0 h^{\varphi} U'_{\theta\varphi} \\ &\quad + \frac{1}{D}\left(U'_{\theta\varphi} U_{\varphi\varepsilon ij} - U'_{\varphi\varphi} U_{\theta\varepsilon ij}\right)\frac{\partial \tilde{u}_i}{\partial a_j}, \\ \delta\varphi &= -\frac{\mu_0}{D} M_s U'_{\theta\varphi} h^{\theta} + \frac{\mu_0}{D} M_s \sin\theta_0 h^{\varphi} U'_{\theta\theta} \\ &\quad + \frac{1}{D}\left(U'_{\theta\varphi} U_{\theta\varepsilon ij} - U'_{\theta\theta} U_{\varphi\varepsilon ij}\right)\frac{\partial \tilde{u}_i}{\partial a_j}, \end{aligned} \tag{24}$$

where $D = U'_{\theta\theta}U'_{\varphi\varphi} - U_{\theta\varphi}{}'2$ and

$$\begin{aligned} U'_{\theta\varphi} &= U_{\theta\varphi} - \mu_0 M_s \cos\theta_0 H_0^{\varphi}, \\ U'_{\varphi\varphi} &= U_{\varphi\varphi} + \mu_0 M_s \sin\theta_0 \left(H_x \cos\varphi_0 + H_y \sin\varphi_0\right), \\ U'_{\theta\theta} &= U_{\theta\theta} + \mu_0 M_s \left(H_x \sin\theta_0 \cos\varphi_0 + H_y \sin\theta_0 \sin\varphi_0 + H_z \cos\theta_0\right). \end{aligned} \tag{25}$$

Introducing these last expressions in the dynamic magnetization, we obtain

$$m_i = \frac{q'_{ikl}}{\mu_0}\frac{\partial u_k}{\partial a_l} + \chi_{il} h_l, \tag{26}$$

with the dynamic susceptibility tensor given by

$$\begin{aligned} \chi_{11} &= \frac{\mu_0 M_s^2}{D}\left(\sin^2\theta_0 \sin^2\varphi_0 U'_{\theta\theta} + \cos^2\theta_0 \cos^2\varphi_0 U'_{\varphi\varphi} \right. \\ &\quad \left. + \frac{1}{2}\sin 2\theta_0 \sin 2\varphi_0 U'_{\theta\varphi}\right), \\ \chi_{12} &= \frac{\mu_0 M_s^2}{2D}\left(-\sin^2\theta_0 \sin 2\varphi_0 U'_{\theta\theta} + \cos^2\theta_0 \sin 2\varphi_0 U'_{\varphi\varphi} \right. \\ &\quad \left. + \sin 2\theta_0 \left(\sin^2\varphi_0 - \cos^2\varphi_0\right) U'_{\theta\varphi}\right), \\ \chi_{13} &= -\frac{\mu_0 M_s^2}{D}\left(\frac{1}{2}\sin 2\theta_0 \cos\varphi_0 U'_{\varphi\varphi} + \sin^2\theta_0 \sin\varphi_0 U'_{\theta\varphi}\right), \\ \chi_{22} &= \frac{\mu_0 M_s^2}{D}\left(\sin^2\theta_0 \cos^2\phi_0 U'_{\theta\theta} + \cos^2\theta_0 \sin^2\phi_0 U'_{\phi\phi} \right. \\ &\quad \left. - \frac{1}{2}\sin 2\theta_0 \sin 2\phi_0 U'_{\theta\phi}\right), \\ \chi_{23} &= \frac{\mu_0 M_s^2}{D}\left(-\frac{1}{2}\sin 2\theta_0 \sin\varphi_0 U'_{\varphi\varphi} + \sin^2\theta_0 \cos\varphi_0 U'_{\theta\varphi}\right), \\ \chi_{33} &= \frac{\mu_0 M_s^2}{D}\sin^2\theta_0 U'_{\varphi\varphi}, \end{aligned} \tag{27}$$

and

$$q'_{mij} = -\frac{b_{ijkl}}{M_s^2}\left(M_{0k}\chi_{lm} + M_{0l}\chi_{km}\right). \tag{28}$$

At this point, a second constitutive equation of the effective piezomagnetic material needs to be found. Starting from the definition of the Piola-Kirchoff stress tensor, *i.e.*, Eq. (4), and of the magnetic-body force, *i.e.*, the second term of the right hand side of Eq. (1), and, as before, using the method of the successive approximations, retaining only the first order dynamic terms, a dynamic stress component can be defined as

$$\sigma_{ij} = C_{ijkl}\frac{\partial u_k}{\partial a_l} + \frac{b_{ijkl}}{M_s^2}\left(M_{0k}m_l + M_{0l}m_k\right) + \mu_0 M_{0l}\delta_{ij}h_l. \tag{29}$$

Introducing in Eq. (29) the expressions (26) of the dynamic magnetization, the dynamic stress tensor becomes

$$\sigma_{ij} = \left(C_{ijkl} + \frac{b_{ijmn}}{\mu_0 M_s^2}\left(M_{0n}q'_{mkl} + M_{0m}q'_{nkl}\right)\right)\frac{\partial u_k}{\partial a_l} + \left(\frac{b_{ijmn}}{M_s^2}\left(M_{0n}\chi_{ml} + M_{0m}\chi_{nl}\right) + \mu_0 M_{0l}\delta_{ij}\right)h_l. \tag{30}$$

Noting that the factor in front of h_l is nothing else than the opposite of the piezomagnetic coefficients $-q_{lij}$ given by

$$q_{lij} = q'_{lij} - \mu_0 M_{0l}\delta_{ij}, \tag{31}$$

we arrive at the piezomagnetic equations

$$\rho_0\frac{\partial^2 u_i}{\partial t^2} = \frac{\partial \sigma_{ij}}{\partial a_j}, \quad \frac{\partial b_i}{\partial a_i} = 0, \tag{32}$$

with

$$\sigma_{ij} = \left(C_{ijkl} + \Delta C_{ijkl}\right)\frac{\partial u_k}{\partial a_l} - q_{lij}h_l, \tag{33}$$

$$b_i = q_{ikl}\frac{\partial u_k}{\partial a_l} + \mu_{il}h_l. \tag{34}$$

Here, the effective magnetic permeability and elastic constants are given by

$$\mu_{il} = \mu_0(\delta_{il} + \chi_{il}), \tag{35}$$

$$C^H_{ijkl} = C_{ijkl} + \Delta C_{ijkl} = C_{ijkl} + \frac{b_{ijmn}}{\mu_0 M_s^2}\left(M_{0n}q'_{mkl} + M_{0m}q'_{nkl}\right). \tag{36}$$

For completeness, all the constants of the effective piezomagnetic material, in the considered case of a crystal with cubic symmetry, are explicitly written as a function of θ_0 and φ_0 in Appendix B.

III. PIEZOMAGNETIC PHONONIC CRYSTAL

In the quasi-static approximation, a magnetic potential φ_m, from which the magnetic field derives, can be introduced

$$h_l = -\partial\varphi_m/\partial a_l. \tag{37}$$

Inserting this magnetic potential in Eqs. (33)–(34), the equivalent piezomagnetic constitutive equations become

$$\sigma_{ij} = \left(C_{ijkl} + \Delta C_{ijkl}\right)\frac{\partial u_k}{\partial a_l} + q_{lij}\frac{\partial \varphi_m}{\partial a_l}, \tag{38}$$

$$b_i = q_{ikl}\frac{\partial u_k}{\partial a_l} - \mu_{il}\frac{\partial \varphi_m}{\partial a_l}. \tag{39}$$

This formulation, similar to the one classically used for piezoelectric materials, enables the direct used of the PWE (Refs. 37 and 38) or FEM (Ref. 39) methods developed for the calculation of phononic crystal characteristics in piezoelectric media.

Let us first recall the basic principles of the PWE method in this case. According to the Bloch-Floquet theorem, the displacement vector and the magnetic potential can be expanded in infinite Fourier series

$$u_i(\boldsymbol{r}, \boldsymbol{t}) = \sum_{\boldsymbol{G}} u^i_{k+G} e^{j(\omega t - \boldsymbol{k}.\boldsymbol{r} - \boldsymbol{G}.\boldsymbol{r})}, \quad \varphi_m(\boldsymbol{r}, \boldsymbol{t}) = \sum_{\boldsymbol{G}} \varphi_{k+G} e^{j(\omega t - \boldsymbol{k}.\boldsymbol{r} - \boldsymbol{G}.\boldsymbol{r})}, \tag{40}$$

where $\boldsymbol{r} = (x, y, z)$ is the vector position, ω is the circular frequency, $\boldsymbol{G}$ are the reciprocal lattice vectors, and $\boldsymbol{k}$ is the wave vector. Moreover, due to the periodicity the material constants $\rho(\boldsymbol{r})$, $C_{ijkl}(\boldsymbol{r})$, $q_{lij}(\boldsymbol{r})$, and $\mu_{ij}(\boldsymbol{r})$ are also expanded as Fourier series

$$\alpha(\boldsymbol{r}) = \sum_{\boldsymbol{G}} \alpha_G e^{-j\boldsymbol{G}.\boldsymbol{r}}. \tag{41}$$

Inserting these expansions, Eqs. (40)–(41), in Eqs. (32) and (38)–(39), using orthogonality property of Fourier series components and collecting terms, yields the following generalized eigenvalue equation[37]

$$\omega^2\tilde{\boldsymbol{R}}\tilde{\boldsymbol{U}} = \Gamma_i\tilde{A}_{il}\Gamma_l\tilde{\boldsymbol{U}}, \tag{42}$$

where $\tilde{\boldsymbol{U}}$ is a vector gathering the Fourier amplitudes of the generalized displacement $\boldsymbol{u} = (u_1, u_2, u_3, \varphi_m)$, $\tilde{\boldsymbol{R}}$, $\tilde{A}_{\text{il}}$ are $4N \times 4N$ matrix involving only material constants, and Γ_i are diagonal matrices involving the wave vector and the Bloch wave vector. The detailed expressions of all these matrices are given in Appendix C. By solving Eq. (42) for ω as a function of the wave vector $\boldsymbol{k}$ in the first Brillouin zone of the considered lattice, the band structures can be calculated. This system of Eq. (42) can also be rewritten as a function of ω and the wave vector direction, leading to a generalized eigenvalue problem for the wave vector $\boldsymbol{k}$. In this case, this formulation can be used to build the complex band structure of the phononic crystal.[50,51]

IV. RESULTS AND DISCUSSION

A. Piezomagnetic equivalent material

In order to compare our results to the ones previously obtained in the literature, we consider piezoelectrically

stiffened elastic constants, as frequently used in piezoelectric materials:[52]

$$\bar{C}_{ijkl} = C^{H}_{ijkl} + \frac{q_{pij} n_p n_q q_{qkl}}{\mu_{mn} n_m n_n}, \tag{43}$$

where n_i are the components of the unit vector in the direction of wave propagation. These stiffened elastic constants, as expressed, depend on the propagation direction, and so cannot be directly used in numerical scheme.

First of all, to validate the obtained results, we consider the case of the influence of an external magnetic field on the propagation of a longitudinal wave along the length of a cubic magnetoelastic rod studied by Eastman.[41] The rod is oriented along the Z axis, and $K_1 = 0$ and $B_i E_{0i} \approx 0$ (see Appendix A). The corresponding stiffened elastic constant $\bar{C}_{33}$, calculated from Eq. (43) with $n_1 = n_2 = 0$ and $n_3 = 1$, is given by

$$\bar{C}_{33} = \mathrm{C}^{H}_{33} + \frac{q^2_{33}}{\mu_{33}} = \mathrm{C}_{33} + \Delta \mathrm{C}_{33} + \frac{q^2_{33}}{\mu_{33}}, \tag{44}$$

where from Eqs. (31), (35), and (36) the piezomagnetic, permeability, and elastic constants are

$$q_{33} = -\frac{2B_1}{H_0}\cos\theta_0 \sin^2\theta_0 - \mu_0 M_s \cos\theta_0, \tag{45}$$

$$\mu_{33} = \frac{\mu_0}{H_0}\left(H_0 + M_s \sin^2\theta_0\right), \tag{46}$$

$$\Delta C_{33} = -\frac{4B_1^2}{\mu_0 M_s H_0}\cos^2\theta_0 \sin^2\theta_0. \tag{47}$$

$H_0 = H_{ext} + H_D$ is the internal magnetic field. Introducing Eqs. (45)–(47) in Eq. (44) we obtain

$$\bar{C}_{33} = C_{33} - \frac{\left(2B_1 - \mu_0 M_s^2\right)^2 \cos^2\theta_0 \sin^2\theta_0}{\mu_0\left(M_s H_0 + M_s^2 \sin^2\theta_0\right)}. \tag{48}$$

It corresponds to the classical observation that the sound velocity is always reduced when magnetoelastic effects are present, leading to an apparent softening of the relevant elastic coefficient. The velocity of the corresponding longitudinal wave is then calculated by $c_l = \sqrt{\bar{C}_{33}/\rho_0}$. This expression corresponds to the magnetic field dependent part given in Table II of Ref. 41. As already pointed out by Eastman,[41] the magnetic body force affects only longitudinal modes and results in B_i appearing in the form $\left(B_i - \mu_0 M_s^2\right)^2$ for longitudinal wave velocities in place of B_i^2 for shear wave velocities.

Now, we consider the case of a cubic magnetoelastic rod, as the one that will be used in the phononic crystal (Fig. 1), with an applied external magnetic field along one of the crystallographic axis. When the magnetic field is applied along Z, parallel to the rod length, the only non zero permeabilities, piezomagnetic constants, and elastic constant variations are

$$\mu_{11} = \mu_{22} = \mu_0\left(1 + \frac{M_s}{H_0 + H_{an} + H_{me}}\right), \ \mu_{33} = \mu_0, \tag{49}$$

$$q_{24} = q_{15} = -\frac{B_2/2}{H_0 + H_{an} + H_{me}}, \tag{50}$$

$$\Delta C_{44} = \Delta C_{55} = -\frac{B_2^2/4}{\mu_0 M_s (H_0 + H_{an} + H_{me})}, \tag{51}$$

where $H_{an} = \frac{2K_1^*}{\mu_0 M_s}$ is the anisotropic field, and $H_{me} = \frac{B_2^2}{4C_{44}\mu_0 M_s}$ is the magnetoelastic field. If the magnetic field is applied along X or Y, the non zero constants of the effective piezomagnetic material are given by Eqs. (49)–(51), simply applying an index permutation. Moreover, when the external magnetic field is applied along the rod axis, *i.e.*, the Z axis, the static demagnetizing field is equal to zero. In the two other directions, the static demagnetizing field is in the same direction as the applied field with an amplitude given by $H_D = -M_s/2$.

The evolutions of the effective elastic coefficients, piezomagnetic constants, and magnetic permeabilities for a Terfenol-D rod as a function of the amplitude of an external magnetic field applied along the rod axis are displayed on Fig. 2. The Terfenol-D parameters used in all the calculations presented in this paper, correspond to the ones of commercially available data: $\rho_0 = 9210$ kg/m^3, $M_s = 800$ kA/m, $K_1 = 4\ 10^5$ J/m^3, $B_1 = b_{1111} = -2\ 10^7$ J/m^3 and $B_2 = 4\, b_{1212} = -3.456\ 10^8$ J/m^3, and $C_{11} = 82$ GPa, $C_{12} = 40$ GPa, and $C_{44} = 48$ GPa. As the external magnetic field is applied in the Z direction, only two elastic coefficients C_{44} and C_{55}, and two piezomagnetic constants q_{24} and q_{15} display strong variations as a function of the magnetic field. The order of magnitude of the predicted transverse elastic coefficient variations are in good agreement with the ones measured in Terfenol-D.[30] These variations can be quantified as follows. The influence of magnetoelastic interaction on spectrum of quasiphonon (*i.e.*,

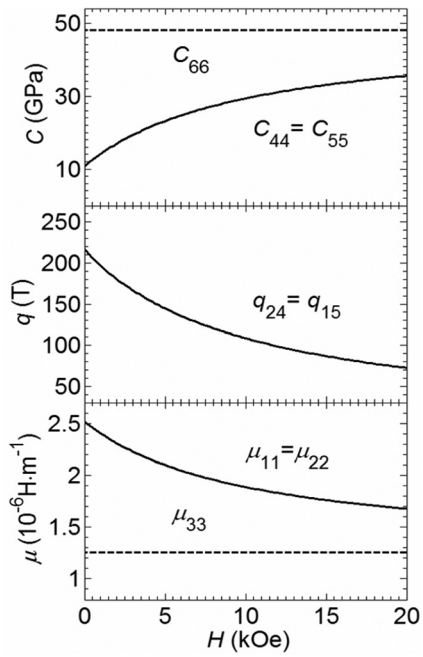

FIG. 2. Evolution of the effective elastic moduli, piezomagnetic constants, and magnetic permeabilities of a Terfenol-D rod as a function of the static external magnetic field applied along the rod axis (Z). The effective elastic and piezomagnetic constants are expressed in Voigt notation.

hybrid magneto-elastic waves), generally small, is characterized by the following dimensionless coupling parameter:[32]

$$\zeta = \frac{\omega_{me}}{\omega_0}, \tag{52}$$

where $\omega_0 = \gamma(H_0 + H_{an} + H_{me})$ is the magnon frequency and $\omega_{me} = \gamma H_{me}$ is the magnetoelastic coupling contribution to the magnon frequency. In a giant magnetostrictive material, for example, in the Terfenol-D rod sample considered here, $H_{me} = 7.5$ kOe, $H_{an} = 2.5$ kOe, and for $H_0 = 10$ kOe, we obtain $\zeta = 0.375$ indicating a high magnetoelastic coupling.

The variations of the diagonal terms of the effective magnetic permeability tensor are also displayed in Fig. 2.

In the considered case of an external magnetic field applied along the Z axis, the only field dependent stiffened elastic constants are

$$\bar{C}_{44} = C_{44}^H + \frac{q_{24}^2 n_2^2}{\mu_{11} n_1^2 + \mu_{22} n_2^2 + \mu_0 n_3^2}, \tag{53}$$

$$\bar{C}_{55} = C_{55}^H + \frac{q_{24}^2 n_1^2}{\mu_{11} n_1^2 + \mu_{22} n_2^2 + \mu_0 n_3^2}, \tag{54}$$

$$\bar{C}_{45} = \frac{q_{24}^2 n_1 n_2}{\mu_{11} n_1^2 + \mu_{22} n_2^2 + \mu_0 n_3^2}, \tag{55}$$

where $\boldsymbol{n} = (n_1, n_2, n_3)$ is a unit vector in the propagation direction. To calculate the velocities of the three propagating waves, in a given direction, the following characteristic equation needs to be solved:[52]

$$\det\left(\Gamma_{il} - \rho_0 V^2\right) = 0, \tag{56}$$

where $\Gamma_{il} = \bar{C}_{ijkl} n_j n_k$ is the Christoffel tensor. Considering elastic waves propagating in the XY plane, *i.e.*, $n_1 = \cos\Phi$, $n_2 = \sin\Phi$ and $n_3 = 0$ where Φ is the angle between the propagation direction and the X axis, the characteristics equation becomes

$$\left(\Gamma_{33} - \rho_0 V^2\right)\left(\left(\Gamma_{11} - \rho_0 V^2\right)\left(\Gamma_{22} - \rho_0 V^2\right) - \Gamma_{12}^2\right) = 0, \tag{57}$$

where

$$\begin{aligned}
\Gamma_{11} &= C_{11}\cos^2\Phi + C_{44}\sin^2\Phi, \\
\Gamma_{22} &= C_{44}\cos^2\Phi + C_{11}\sin^2\Phi, \\
\Gamma_{33} &= \bar{C}_{55}\cos^2\Phi + \bar{C}_{44}\sin^2\Phi + 2\bar{C}_{45}\cos\Phi\sin\Phi \\
&= C_{44} - \frac{B_2^2/4}{\mu_0 M_s (M_s + H_0 + H_{an} + H_{me})}.
\end{aligned} \tag{58}$$

Here only the component Γ_{33} of the Christoffel tensor is field dependent. So, only the decoupled out of plane transverse mode, with velocity $\sqrt{\Gamma_{33}/\rho_0}$, depends on the external magnetic field. The slowness polar diagrams calculated for elastic waves propagating in the XY plane, using the effective piezomagnetic material properties are shown in Fig. 3 for three increasing values of the amplitude of the external magnetic field: 1 kOe (dashed line), 10 kOe (dotted line), and 20 kOe (solid line). In this configuration, only the out of plane transverse wave, propagating with the velocity and with displacement directed along the applied static magnetic field, is coupled to this magnetic field.

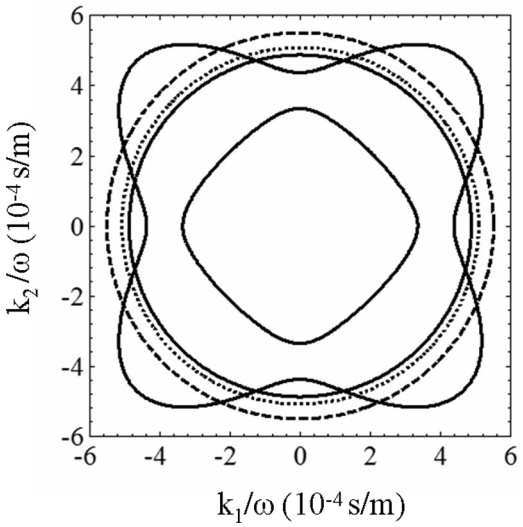

FIG. 3. Slowness polar diagram for propagation in a Terfenol-D rod with a static external magnetic field, applied along the rod axis (Z), of 1 kOe (dashed line), 10 kOe (dotted line), and 20 kOe (solid line).

Considering now a magnetic field applied in a direction perpendicular to the Terfenol-D rod, the evolution of the parameters of the effective piezomagnetic material as a function of the amplitude of the external magnetic field are presented in Fig. 4. In this configuration, elastic waves

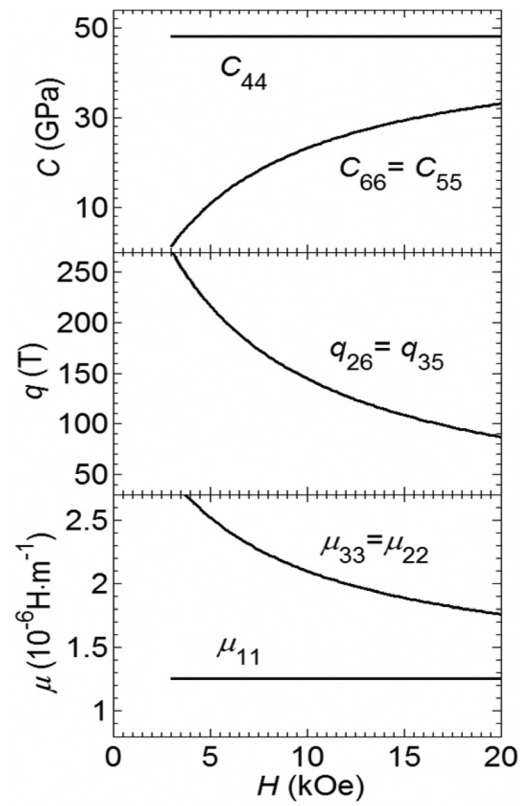

FIG. 4. Evolution of the effective elastic moduli, piezomagnetic constants, and magnetic permeabilities of a Terfenol-D rod as a function of the static external magnetic field applied along the X axis. The effective elastic and piezomagnetic constants are expressed in Voigt notation.

propagating in the *XY* plane are described by the same characteristics equation, *i.e.*, Eq. (57), with now

$$\begin{aligned}\Gamma_{11} &= C_{11}\cos^2\Phi + \bar{C}_{66}\sin^2\Phi,\\ \Gamma_{22} &= \bar{C}_{66}\cos^2\Phi + C_{11}\sin^2\Phi,\\ \Gamma_{33} &= \bar{C}_{55}\cos^2\Phi + C_{44}\sin^2\Phi,\\ \Gamma_{12} &= (C_{12}+\bar{C}_{66})\cos\Phi\sin\Phi,\end{aligned} \tag{59}$$

and

$$\bar{C}_{55} = C_{55} - \frac{B_2^2/4}{\mu_0 M_s(H_0 + H_{an} + H_{me})}, \tag{60}$$

$$\bar{C}_{66} = C_{55} - \frac{B_2^2/4}{\mu_0 M_s\left(H_0 + H_{an} + H_{me} + M_s\sin^2\Phi\right)}. \tag{61}$$

Contrary to the previous case, all the Christoffel tensor components are now field dependent. As shown on Fig. 5, displaying the slowness polar diagrams for an external field of 4 kOe (dashed line), 10 kOe (dotted line), and 20 kOe (solid line), this leads to the fact that all the modes are now affected by the magnetic field, even if the influence on the quasi-longitudinal mode is still low.

Moreover, the induced velocities variations of the transverse waves, both in plane and out of plane, become very large for propagation in the *X* direction, due to the presence of a magnetic spin reorientation transition (SRT). It is well known that the magnetoelastic coupling can become significant near a SRT if the magnetic mode of frequency ω_0 that interacts with the sound is a soft mode, *i.e.*, a mode with $\omega_0 = \omega_{\text{me}}$ at the SRT, leading to $\zeta = 1$ at the transition. Starting from a high amplitude, around 20 k0e, external magnetic field oriented along the X axis, and then decreasing its amplitude, the ground state $\boldsymbol{M}_0//\boldsymbol{H}_{ext}//\text{X}$ is stable under the condition:[32]

$$\frac{2K_1^*}{\mu_0 M_s} + H_0 = H_{an} + H_0 \geq 0, \tag{62}$$

where K_1^* is given by Eq. (21). At the SRT, *i.e.*, when $H_{an} + H_0 = 0$ or $H_{ext} = -H_{an} - H_D$, the equilibrium state suddenly changes, as shown on Fig. 6. Note that $\varphi_0 = 0$ for all values of the external applied field. For the considered Terfenol-D sample, the SRT corresponds to $H_{ext} = 2.56$ kOe. Close to the SRT, *e.g.*. for $H_{ext} = 4$ kOe, for a propagation along the external magnetic field direction ($\Phi = 0$), the phase velocity of the transverse waves, $c_t = \sqrt{\bar{C}_{55}/\rho_0}$, tends to zero. In the other hand, when the propagation is perpendicular to the external field direction, only the in plane transverse wave velocity shows a slight variation as a function of the magnetic field amplitude. The difference between these two cases arises from the existence of a dynamic dipole field $h = M_s\sin^2\Phi$ created by the magnetoelastic waves propagation. As shown in Eq. (61), when $\boldsymbol{k}$ // $\boldsymbol{M}_0$ // X the dynamic dipole field $\boldsymbol{h}$ becomes zero. But with increasing angle between $\boldsymbol{k}$ and $\boldsymbol{M}_0$, the dipole field increases up to $\boldsymbol{M}_s$ when $\boldsymbol{k}$ becomes perpendicular to $\boldsymbol{M}_0$. This field is added to the static demagnetizing field leading to

$$\zeta = \frac{H_{me}}{(H_0 + M_s + H_{an} + H_{me})}, \tag{63}$$

and the magnetoelastic coupling parameter decreases even at SRT where $\zeta_{\text{SRT}} \approx 0.43$ for Terfenol-D. So the long-range dipole interaction can considerably weaken the magnetoelastic coupling at the SRT for waves propagating in an arbitrary direction.

To conclude this part, we consider the results obtained in the rotationally invariant theory,[32] when the external magnetic field is applied along the *Z* axis. The term B_2 in the field dependent variations of the stiffened elastic constant $\bar{C}_{44}$ is replaced by $B_2 \pm K_{1me}$ where

$$K_{1me} = K_1 - \frac{B_1 B_2}{4(C_{11} - C_{12})}.$$

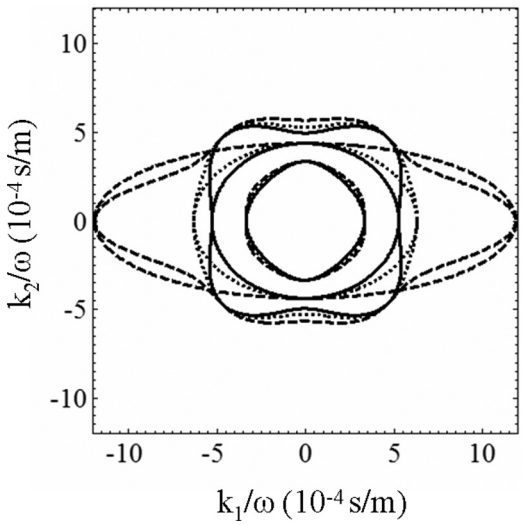

FIG. 5. Slowness polar diagram for propagation in a Terfenol-D rod with a static external magnetic field, applied along the X axis, of 4 kOe (dashed line), 10 kOe (dotted line), and 20 kOe (solid line).

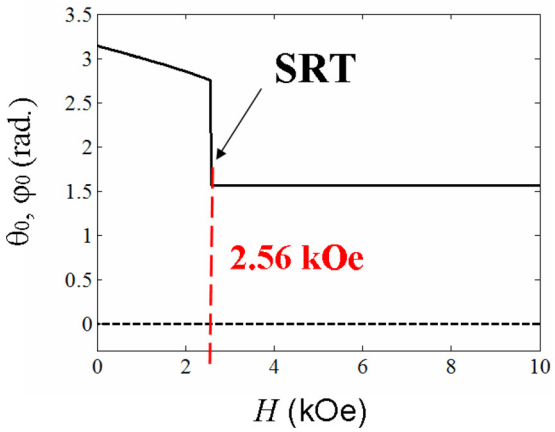

FIG. 6. (Color online) Evolution of the equilibrium state (θ_0, φ_0) for an external static magnetic field of decreasing amplitude applied along the X axis: θ_0 solid line and φ_0 dashed line. A spin reorientation transition (SRT) appears at $H_{ext} = 2.56$ kOe.

The ± sign depends on the wave propagation direction $\boldsymbol{k}$: + if $\boldsymbol{k} \perp \boldsymbol{M}_0$ and - if $\boldsymbol{k} \parallel \boldsymbol{M}_0$. In the considered case of Terfenol-D rod, $K_{1me} \approx 3.59 \times 10^5$ J/m^3 is negligible in comparison with $B_2 \approx 3.456 \times 10^8$ J/m^3. This last point justifies our choice to neglect the effects introduced by the consideration of the complete rotationally invariant theory.

B. Piezomagnetic phononic crystal

We study now the influence of the introduction of a magnetoelastic medium on the properties of phononic crystals. The calculations have been made for square and triangular lattices of Terfenol-D square rods of section $d = 1$ mm embedded in an epoxy matrix. The matrix is constituted of epoxy resin, considered as isotropic and with the following parameters: $\rho_0 = 1142$ kg/m^3, $C_{11} = 7.54$ GPa, and $C_{44} = 1.48$ GPa. 441 plane waves have been used in the PWE calculation of the band structure. Comparison with FEM results has confirmed the convergence of the Fourier series.

The demagnetizing field depends only on the magnetization and the geometrical shape of the sample. Up to now, the demagnetizing contribution, as described by Eqs. (16) and (19), has been calculated for an isolated rod of infinite length. At this point, it becomes important to estimate the influence of the magnetostatic fields of the surrounding magnetoelastic rods on the demagnetizing field, when the phononic crystal is constructed. In fact, it has been demonstrated by Ignatchenko *et al.*[53] that the average magnetostatic field inside a rod in a periodic arrangement of infinitely long square rods is

$$\langle H_D \rangle = \frac{-M_s}{2}(1-f), \tag{64}$$

where f is the filling factor. This equation is also valid for a periodic array of magnetoelastic rods embedded in a non magnetic matrix. So the demagnetizing field is decreased by a factor $(1-f)$ in the phononic crystal configuration in comparison to an isolated rod. This shifts the value of the external magnetic field corresponding to the SRT by a factor of $-f M_s/2$. Moreover, it can be shown that even in the real case where the rods have a finite length h, Eq. (64) remains a very good approximation as soon as $h/a \approx 1.5$, where a is the lattice period.[54] When $\boldsymbol{M}_0 \parallel Z$, where Z is along the rod length, the neighboring square rods have no influence, and the demagnetizing field remains equal to zero.

1. Square lattice phononic crystals

We study the evolution of the band structure of square lattice phononic crystals, as a function of the amplitude and the orientation of the external magnetic field, induced by the variations of the effective parameters of the Terfenol-D rods shown in Figs. 2–5. The band structures displayed in Fig. 7 give a typical example of the magnetic field influence when applied along the rod axis. With a filling factor $f = (d/a)^2 = 0.35$ and an applied field $H_{ext} = 3$ kOe, the phononic crystal possesses an absolute bandgap in the 0–1 MHz frequency

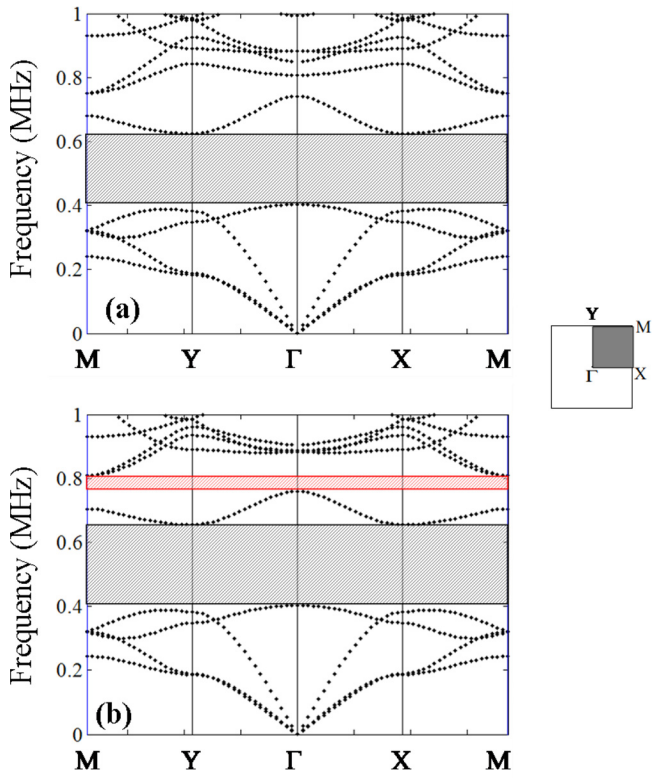

FIG. 7. (Color online) Band structure of a square lattice of Terfenol-D square rods with a filling factor $f = (d/a)^2 = 0.35$, embedded in an epoxy matrix for two applied static magnetic fields along the rod axis Z: (a) $H_{ext} = 3$ kOe and (b) $H_{ext} = 10$ kOe.

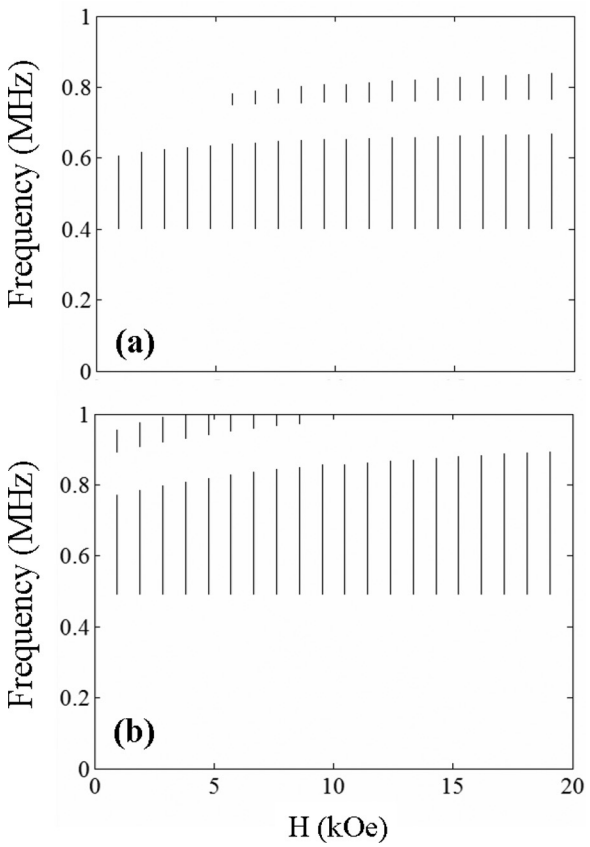

FIG. 8. Evolution of the absolute elastic band gaps of a square lattice of Terfenol D square rods embedded in an epoxy matrix as a function of the amplitude of the applied static external magnetic field along the rod axis Z, for a filling factor (a) $f = 0.35$ and (b) $f = 0.5$.

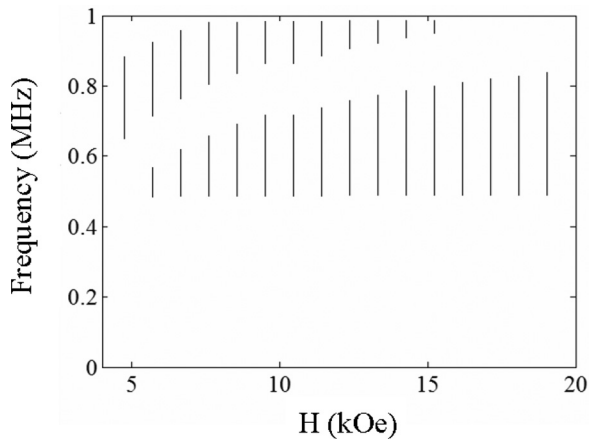

FIG. 9. Evolution of the absolute elastic band gaps of a square lattice of Terfenol-D square rods with a filling factor $f = 0.5$, embedded in an epoxy matrix, as a function of the amplitude of the applied static external magnetic field along the X axis perpendicular to the rod axis.

range, as shown in Fig. 7(a). When the external field is increased to 10 kOe, a second absolute bandgap, ranging from approximately 0.76 to 0.8 MHz, appears (Fig. 7(b)). Moreover, the frequency range of the first absolute band gap is slightly increased. More precisely, the application of a magnetic field with an amplitude higher than 6 kOe increases the bandwidth of the bandgap, and opens a second one in the 0-1 MHz frequency range, as shown in Fig. 8(a). So, elastic waves are evanescent waves in this phononic crystal at 0.8 MHz when the field becomes higher than 6 kOe. When the filling factor is increased to 0.5, as shown in Fig. 8(b), the process is inverted: The second absolute band gap disappears when the amplitude of the external magnetic field is increased. In both cases, the phononic crystal behaves as a switch controlled without any contact by an external applied magnetic field. Nevertheless, in this case, where the magnetic field is applied

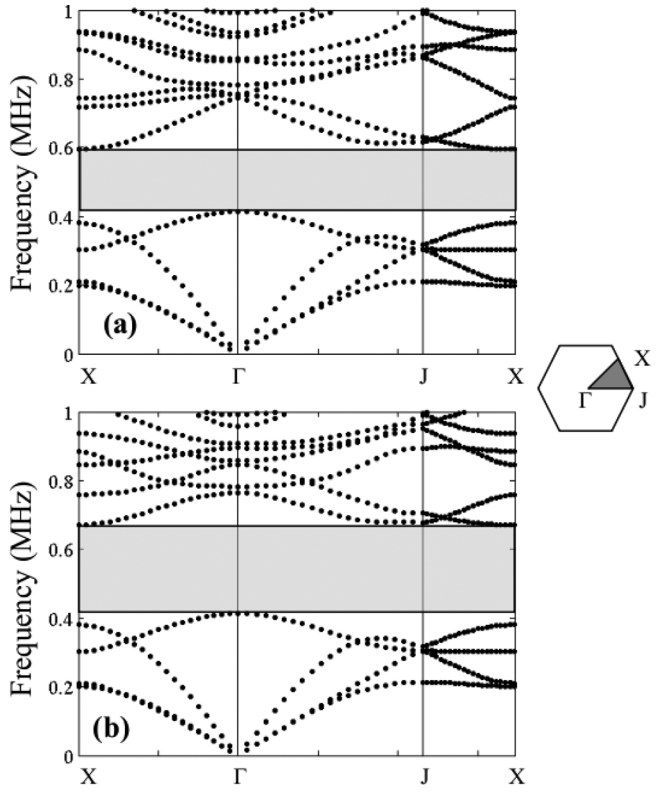

FIG. 11. Band structure of a triangular lattice of Terfenol-D square rods with a filling factor $f = (d/a)^2 = 0.35$, embedded in an epoxy matrix for two applied static magnetic fields along the rod axis Z: (a) $H_{ext} = 3$ kOe and (b) $H_{ext} = 10$ kOe.

along the rod axis, the band gap width variation remains lower than 25%. Moreover, a careful look at the band structures of Fig. 7 has shown that only modes polarized along Z are coupled to the external field.[29]

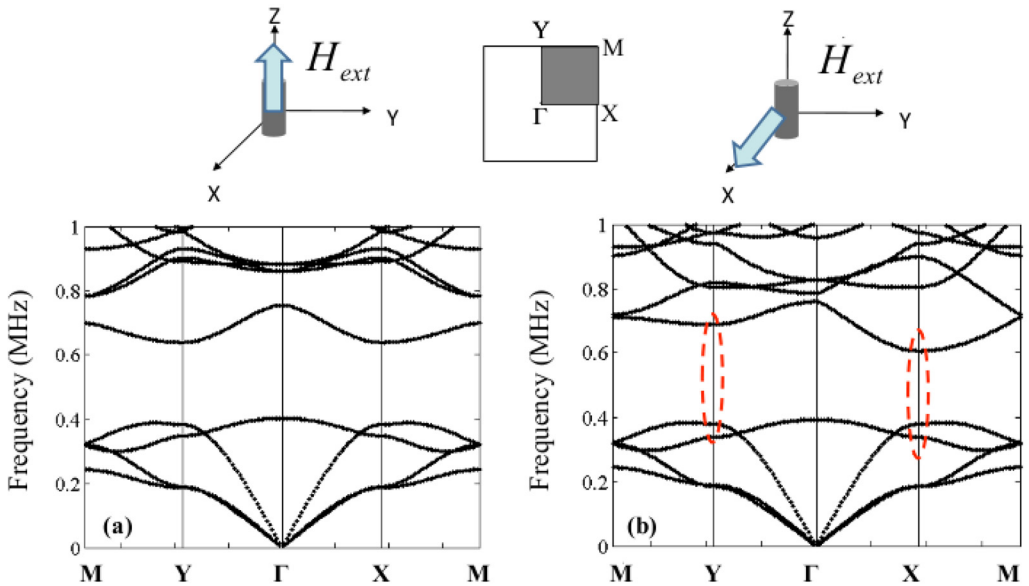

FIG. 10. (Color online) Band structure of a square lattice of Terfenol-D square rods with a filling factor $f = (d/a)^2 = 0.35$, embedded in an epoxy matrix for an applied static magnetic field $H_{ext} = 10$ kOe (a) along the rod axis Z and (b) along the X axis, perpendicular to the rod axis. The inset shows the irreducible Brillouin zone of the square array. The dashed ellipses highlight the strong anisotropy induced by the external static magnetic field.

When the magnetic field is applied perpendicularly to the Terfenol-D rod axis, the absolute band gap evolution displayed in Fig. 9 shows more important variations than in the previous considered case where the magnetic field was along the rod axis. This can be directly linked to the SRT described in the preceding section. The calculations have been made for decreasing external magnetic field amplitude down to 4 kOe, not too close to the SRT. Indeed, below and close to the SRT, the used assumption of uniformerly oriented magnetization becomes doubtful.

In the previous examples, the band structure modifications were obtained by varying the amplitude of the applied magnetic field. Another way to induce such modifications is by changing the field direction, keeping the amplitude constant. As shown in Fig. 10, the band structure of a square lattice of Terfenol-D square rods embedded in an epoxy matrix with a filling factor $f=0.35$ can become strongly anisotropic only by switching the direction of the applied field from the Z axis to the X axis, as highlighted by the dashed ellipses. Indeed, it has been demonstrated in Sec. IV A that close to the SRT the elastic behavior of the magnetoelastic medium becomes highly anisotropic, due to the dynamic dipole field.

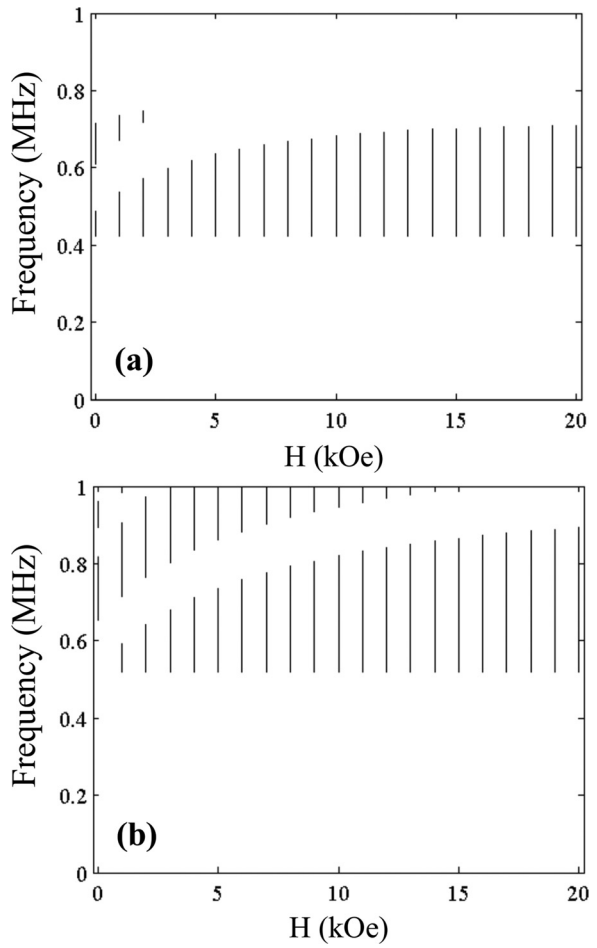

FIG. 12. Evolution of the absolute elastic band gaps of a triangular lattice of Terfenol D square rods embedded in an epoxy matrix as a function of the amplitude of the applied static external magnetic field along the rod axis Z, for a filling factor (a) $f=0.35$ and (b) $f=0.5$.

2. Triangular lattice phononic crystals

We study now the evolution of the band structure of triangular lattice phononic crystals, along the contours of the first irreducible Brillouin zone, as a function of the amplitude of an external magnetic field applied along the rod axis. As for square lattice case, the band structure of a triangular lattice of Terfenol-D square rods, with a filling factor of 0.35, embedded in an epoxy matrix is considerably modified when the amplitude H_{ext} is changed from 3 kOe to 10 kOe, as shown in Fig. 11. Here, in the 0 to 1 MHz frequency range, only one absolute bandgap appears, and its width increases with the external magnetic field amplitude. Comparatively to the square lattice case, this band gap width increase is larger, here, for a triangular lattice.

Figure 12 displays the evolution of the absolute band gaps, for the same triangular lattice magnetoelastic phononic crystal, as a function of the amplitude of the applied external field along the rod axis for two filling factor 0.35 (a) and 0.5 (b). Here, for both filling factors the second absolute band gap disappears when the amplitude of the external magnetic field is increased, even if the closing amplitude is considerably higher, 16 kOe in place of 3 kOe, when $f=0.5$. Moreover, the increase of the width of the first absolute band gap with the external magnetic field amplitude is largely higher for triangular lattices than for square ones. For example, when $f=0.5$ the width of the first gap, ranging from approximately 0.52 to 0.59 MHz when $H_{ext}=1$ kOe, is multiplied by a factor of 5 when the magnetic field is increased up to 20 kOe (where the gap ranges from 0.52 to 0.89 MHz). These variations are in the same order of magnitude as the ones obtained in the case of the square lattice magnetoelastic phononic crystal, considered in the previous paragraph, when we are close to a SRT.

V. CONCLUSION

We have demonstrated the feasibility of tuning the band structure of a magnetoelastic phononic crystal constituted of rods of magnetoelastic material embedded in an epoxy matrix by applying an external magnetic field. Indeed, the elastic properties of magneto-elastic material are very sensitive to its magnetic state and on the applied magnetic field. For instance, in giant magnetostrictive material, such as Terfenol-D, we have shown that this dependence can lead to more than 50% variation of some of the elastic constants. Moreover, the use of giant magnetostriction is not the only means to obtain large elastic properties variations in magnetic materials, and we have also considered spin-reorientation phase transitions effects. In both cases, band structures have been calculated with a plane wave expansion method that accounts for coupling between the elastic behavior and the magnetic field through the development of an equivalent piezomagnetic material of a polarized ferromagnet, with elastic, piezomagnetic, and magnetic permeability effective tensors. The introduction of a magnetoelastic constituent opens the possibility of easy controllability of the properties of a phononic crystal without any contact. More specifically one can achieve additional functionalities such as the switching of transmission in a defined frequency range.

APPENDIX A: EQUILIBRIUM STRAINS

The equilibrium strains E_{ij}^0, obtained by minimization of the energy U_T, can be shown to be[47]

$$E_{11}^0 = -h_1\alpha_1^{02} + C = -h_1\sin^2\theta_0\cos^2\varphi_0 + C, \tag{A1}$$

$$E_{22}^0 = -h_1\alpha_2^{02} + C = -h_1\sin^2\theta_0\sin^2\varphi_0 + C, \tag{A2}$$

$$E_{33}^0 = -h_1\alpha_3^{02} + C = -h_1\cos^2\theta_0 + C, \tag{A3}$$

$$E_{23}^0 = -h_2\alpha_2^0\alpha_3^0 = -\frac{h_2}{2}\sin2\theta_0\sin\varphi_0, \tag{A4}$$

$$E_{13}^0 = -h_2\alpha_1^0\alpha_3^0 = -\frac{h_2}{2}\sin2\theta_0\cos\varphi_0, \tag{A5}$$

$$E_{12}^0 = -h_2\alpha_1^0\alpha_2^0 = -\frac{h_2}{2}\sin^2\theta_0\sin2\varphi_0, \tag{A6}$$

where

$$h_1 = \frac{B_1}{C_{11} - C_{12}}, \tag{A7}$$

$$h_2 = \frac{B_2}{4C_{44}}, \tag{A8}$$

and

$$C = \frac{B_1C_{12}}{(C_{11} - C_{12})(C_{11} + 2C_{12})}. \tag{A9}$$

APPENDIX B: EFFECTIVE CONSTANTS

The effective magnetic permeability μ_{ij}, piezomagnetic coupling coefficient q_{iJ}, and elastic constant correction ΔC_{IJ} for a cubic system are given in Voigt notation (where i, $j = 1, 2, 3$ and $I, J = 1, 2, \ldots 6$) by:

$$\mu_{11} = \mu_0(1 + \chi_{11})$$

$$\mu_{12} = \mu_0\chi_{12}$$

$$\mu_{13} = \mu_0\chi_{13}$$

$$\mu_{22} = \mu_0(1 + \chi_{22})$$

$$\mu_{23} = \mu_0\chi_{23}$$

$$\mu_{33} = \mu_0(1 + \chi_{33})$$

$$q_{11} = -\frac{2B_1}{M_s}\sin\theta_0\cos\varphi_0\chi_{11} - \mu_0M_s\sin\theta_0\cos\varphi_0$$

$$q_{12} = -\frac{2B_1}{M_s}\sin\theta_0\sin\varphi_0\chi_{12} - \mu_0M_s\sin\theta_0\cos\varphi_0$$

$$q_{13} = -\frac{2B_1}{M_s}\cos\theta_0\chi_{13} - \mu_0M_s\sin\theta_0\cos\varphi_0$$

$$q_{14} = -\frac{B_2}{2M_s}(\sin\theta_0\sin\varphi_0\chi_{13} + \cos\theta_0\chi_{12})$$

$$q_{15} = -\frac{B_2}{2M_s}(\sin\theta_0\cos\varphi_0\chi_{13} + \cos\theta_0\chi_{11})$$

$$q_{16} = -\frac{B_2}{2M_s}(\sin\theta_0\cos\varphi_0\chi_{12} + \sin\theta_0\sin\varphi_0\chi_{11}),$$

$$q_{21} = -\frac{2B_1}{M_s}\sin\theta_0\cos\varphi_0\chi_{12} - \mu_0M_s\sin\theta_0\sin\varphi_0,$$

$$q_{22} = -\frac{2B_1}{M_s}\sin\theta_0\sin\varphi_0\chi_{22} - \mu_0M_s\sin\theta_0\sin\varphi_0,$$

$$q_{23} = -\frac{2B_1}{M_s}\cos\theta_0\chi_{23} - \mu_0M_s\sin\theta_0\sin\varphi_0,$$

$$q_{24} = -\frac{B_2}{2M_s}(\sin\theta_0\sin\varphi_0\chi_{23} + \cos\theta_0\chi_{22}),$$

$$q_{25} = -\frac{B_2}{2M_s}(\sin\theta_0\cos\varphi_0\chi_{23} + \cos\theta_0\chi_{12}),$$

$$q_{26} = -\frac{B_2}{2M_s}(\sin\theta_0\cos\varphi_0\chi_{22} + \sin\theta_0\sin\varphi_0\chi_{12}),$$

$$q_{31} = -\frac{2B_1}{M_s}\sin\theta_0\cos\varphi_0\chi_{13} - \mu_0M_s\cos\theta_0,$$

$$q_{32} = -\frac{2B_1}{M_s}\sin\theta_0\sin\varphi_0\chi_{23} - \mu_0M_s\cos\theta_0,$$

$$q_{33} = -\frac{2B_1}{M_s}\cos\theta_0\chi_{33} - \mu_0M_s\cos\theta_0,$$

$$q_{34} = -\frac{B_2}{2M_s}(\sin\theta_0\sin\varphi_0\chi_{33} + \cos\theta_0\chi_{23}),$$

$$q_{35} = -\frac{B_2}{2M_s}(\sin\theta_0\cos\varphi_0\chi_{33} + \cos\theta_0\chi_{13}),$$

$$q_{36} = -\frac{B_2}{2M_s}(\sin\theta_0\cos\varphi_0\chi_{23} + \sin\theta_0\sin\varphi_0\chi_{13}),$$

$$\Delta C_{11} = -\frac{4B_1^2}{M_s^2}\sin^2\theta_0\cos^2\varphi_0\chi_{11},$$

$$\Delta C_{12} = -\frac{4B_1^2}{M_s^2}\sin^2\theta_0\cos\varphi_0\sin\varphi_0\chi_{12},$$

$$\Delta C_{13} = -\frac{4B_1^2}{M_s^2}\cos\theta_0\sin\theta_0\cos\varphi_0\chi_{13},$$

$$\Delta C_{14} = -\frac{B_1B_2}{M_s^2}\sin\theta_0\cos\varphi_0(\sin\theta_0\sin\varphi_0\chi_{13} + \cos\theta_0\chi_{12}),$$

$$\Delta C_{15} = -\frac{B_1B_2}{M_s^2}\sin\theta_0\cos\varphi_0(\sin\theta_0\cos\varphi_0\chi_{13} + \cos\theta_0\chi_{11}),$$

$$\Delta C_{16} = -\frac{B_1B_2}{M_s^2}\sin\theta_0\cos\varphi_0(\sin\theta_0\cos\varphi_0\chi_{12} + \sin\theta_0\sin\varphi_0\chi_{11}),$$

$$\Delta C_{22} = -\frac{4B_1^2}{M_s^2}\sin^2\theta_0\sin^2\varphi_0\chi_{22},$$

$$\Delta C_{23} = -\frac{4B_1^2}{M_s^2}\sin\theta_0\cos\theta_0\sin\varphi_0\chi_{23},$$

$$\Delta C_{24} = -\frac{B_1B_2}{M_s^2}\sin\theta_0\sin\varphi_0(\sin\theta_0\sin\varphi_0\chi_{23} + \cos\theta_0\chi_{22}),$$

$$\Delta C_{25} = -\frac{B_1B_2}{M_s^2}\sin\theta_0\sin\varphi_0(\sin\theta_0\cos\varphi_0\chi_{23} + \cos\theta_0\chi_{12}),$$

$$\Delta C_{26} = -\frac{B_1B_2}{M_s^2}\sin\theta_0\sin\varphi_0(\sin\theta_0\cos\varphi_0\chi_{22} + \sin\theta_0\sin\varphi_0\chi_{12}),$$

$$\Delta C_{33} = -\frac{4B_1^2}{M_s^2}\cos\theta_0^2\chi_{33},$$

$$\Delta C_{34} = -\frac{B_1B_2}{M_s^2}\cos\theta_0(\sin\theta_0\sin\varphi_0\chi_{33} + \cos\theta_0\chi_{23}),$$

$$\Delta C_{35} = -\frac{B_1B_2}{M_s^2}\cos\theta_0(\sin\theta_0\cos\varphi_0\chi_{33} + \cos\theta_0\chi_{13}),$$

$$\Delta C_{36} = -\frac{B_1B_2}{M_s^2}\cos\theta_0(\sin\theta_0\cos\varphi_0\chi_{23} + \sin\theta_0\sin\varphi_0\chi_{13}),$$

$$\Delta C_{44} = -\frac{B_2^2}{4M_s^2}(\sin^2\theta_0\sin^2\varphi_0\chi_{33} + \cos^2\theta_0\chi_{22} + 2\cos\theta_0\sin\theta_0\sin\varphi_0\chi_{23}),$$

$$\Delta C_{45} = -\frac{B_2^2}{4M_s^2}(\sin^2\theta_0\cos\varphi_0\sin\varphi_0\chi_{33} + \cos^2\theta_0\chi_{12} + \cos\theta_0\sin\theta_0\cos\varphi_0\chi_{23} + \cos\theta_0\sin\theta_0\sin\varphi_0\chi_{13}),$$

$$\Delta C_{46} = -\frac{B_2^2}{4M_s^2}(\sin^2\theta_0\cos\varphi_0\sin\varphi_0\chi_{23} + \sin^2\theta_0\sin^2\varphi_0\chi_{13} + \cos\theta_0\sin\theta_0\cos\varphi_0\chi_{22} + \cos\theta_0\sin\theta_0\sin\varphi_0\chi_{12}),$$

$$\Delta C_{55} = -\frac{B_2^2}{4M_s^2}(\sin^2\theta_0\cos^2\varphi_0\chi_{33} + \cos^2\theta_0\chi_{11} + 2\cos\theta_0\sin\theta_0\cos\varphi_0\chi_{13}),$$

$$\Delta C_{56} = -\frac{B_2^2}{4M_s^2}(\sin^2\theta_0\cos\varphi_0\sin\varphi_0\chi_{13} + \sin^2\theta_0\cos^2\varphi_0\chi_{23} + \cos\theta_0\sin\theta_0\cos\varphi_0\chi_{12} + \cos\theta_0\sin\theta_0\sin\varphi_0\chi_{11}),$$

$$\Delta C_{66} = -\frac{B_2^2}{4M_s^2}(\sin^2\theta_0\cos^2\varphi_0\chi_{22} + \sin^2\theta_0\cos^2\varphi_0\chi_{11} + 2\sin^2\theta_0\sin\varphi_0\cos\varphi_0\chi_{12}),$$

where the components of the susceptibility tensor χ_{ij} are given by Eqs. (27) with

$$\begin{aligned}U'_{\theta\theta} =& \mu_0 M_s\left(H_x\sin\theta_0\cos\varphi_0 + H_y\sin\theta_0\sin\varphi_0 + H_z\cos\theta_0\right)\\ &+K_1\left(2\cos4\theta_0 + 3\sin^2 2\varphi_0\cos^2\theta_0\sin^2\theta_0 - \sin^2 2\varphi_0\sin^4\theta_0\right)\\ &+2B_1\left(E_{11}^0\cos2\theta_0\cos^2\varphi_0 + E_{22}^0\cos2\theta_0\sin^2\varphi_0\right.\\ &\left.-E_{33}^0\cos2\theta_0\right) + B_2\left(E_{12}^0\cos2\theta_0\sin2\varphi_0 - 2E_{23}^0\sin2\theta_0\sin\varphi_0\right.\\ &\left.-2E_{13}^0\sin2\theta_0\cos\varphi_0\right),\end{aligned} \tag{B1}$$

$$\begin{aligned}U'_{\varphi\varphi} =& \mu_0 M_s\left(H_x\sin\theta_0\cos\varphi_0 + H_y\sin\theta_0\sin\varphi_0\right)\\ &+2K_1\left(\sin^4\theta_0\cos4\varphi_0\right)\\ &+2B_1\left(-E_{11}^0\sin^2\theta_0\cos2\varphi_0 + E_{22}^0\sin^2\theta_0\cos2\varphi_0\right)\\ &-B_2\left(2E_{12}^0\sin^2\theta_0\sin2\varphi_0 + E_{23}^0\sin\theta_0\cos\theta_0\sin\varphi_0\right.\\ &\left.+E_{13}^0\sin\theta_0\cos\theta_0\cos\varphi_0\right),\end{aligned} \tag{B2}$$

$$\begin{aligned}U'_{\theta\varphi} =& \mu_0 M_s\left(H_x\cos\theta_0\sin\varphi_0 - H_y\cos\theta_0\cos\varphi_0\right)\\ &+2K_1\left(\sin^3\theta_0\cos\theta_0\sin4\varphi_0\right)\\ &+B_1\left(-E_{11}^0\sin2\theta_0\sin2\phi_0 + E_{22}^0\sin2\theta_0\sin2\phi_0\right)\\ &+B_2\left(E_{12}^0\sin2\theta_0\cos2\varphi_0 + E_{23}^0\cos2\theta_0\cos\varphi_0\right.\\ &\left.-E_{13}^0\cos2\theta_0\sin\varphi_0\right).\end{aligned} \tag{B3}$$

APPENDIX C: MATRICES ELEMENTS

The elements of matrices used in the generalized eigenvalue equation, Eq. (42), are

$$\tilde{A}_{il} = \begin{bmatrix} A_{il}^0 & A_{il}^{G^1-G^2} & \cdots & A_{il}^{G^1-G^N} \\ A_{il}^{G^2-G^1} & A_{il}^0 & \cdots & A_{il}^{G^2-G^N} \\ \vdots & \vdots & \ddots & \vdots \\ A_{il}^{G^N-G^1} & A_{il}^{G^N-G^2} & \cdots & A_{il}^0 \end{bmatrix}, \tag{C1}$$

$$\tilde{R} = \begin{bmatrix} \rho_0 I_p & \rho_{G^1-G^2} I_p & \cdots & \rho_{G^1-G^N} I_p \\ \rho_{G^2-G^1} I_p & \rho_0 I_p & \cdots & \rho_{G^2-G^N} I_p \\ \vdots & \vdots & \ddots & \vdots \\ \rho_{G^N-G^1} I_p & \rho_{G^N-G^2} I_p & \cdots & \rho_0 I_p \end{bmatrix}, \tag{C2}$$

$$\Gamma_i = \begin{bmatrix} \left(k_i + G_i^1\right) I_4 & 0 & \cdots & 0 \\ 0 & \left(k_i + G_i^2\right) I_4 & \cdots & 0 \\ \vdots & \vdots & \ddots & \vdots \\ 0 & 0 & \cdots & \left(k_i + G_i^N\right) I_4 \end{bmatrix}, \tag{C3}$$

where $A_{il}^G(j,\,k) = C_{ijkl}^G$, $A_{il}^G(j,\,4) = q_{lij}^G$, $A_{il}^G(4,\,k) = q_{ikl}^G$, $A_{il}^G(4,\,4) = -\mu_{il}^G$ with $(j,\,k) \in [1,3]$.[2]

[1]M. Sigalas and E. Economou, Solid State Commun. **86**, 141 (1993).
[2]M. S. Kushwaha, P. Halevi, L. Dobrzynski, and B. Djafari-Rouhani, Phys. Rev. Lett. **71**, 2022 (1993).
[3]A. Khelif, B. Djafari-Rouhani, J. O. Vasseur, P. A. Deymier, P. Lambin, and L. Dobrzynski, Phys. Rev. B **65**, 174308 (2002).
[4]T. Miyashita and C. Inoue, Jpn. J. Appl. Phys., Part 1 **40**, 3488 (2001).

[5]H. Chandra, P. A. Deymier, and J. O. Vasseur, Phys. Rev. B **70**, 054302 (2004).
[6]R. H. Olsson III, I. F. El-Kady, M. F. Su, M. R. Tuck, and J. G. Fleming, Sensors Actuators A **145–146**, 87 (2008).
[7]Y. Pennec, B. Djafari-Rouhani, J. O. Vasseur, A. Khelif, and P. A. Deymier, Phys. Rev. E **69**, 046608 (2004).
[8]R. H. Olsson III and I. El-Kady, Meas. Sci. Technol. **20**, 012002 (2009).
[9]I. El-Kady, R. H. Olsson III, and J. G. Fleming, Appl. Phys. Lett. **92**, 233504 (2008).
[10]S. Mohammadi, A. A. Eftekhar, W. D. Hunt, and A. Adibi, Appl. Phys. Lett. **94**, 051906 (2009).
[11]T.-T. Wu, W.-S. Wang, J.-H. Sun, J.-C. Hsu, and Y.-Y. Chen, Appl. Phys. Lett. **94**, 101913 (2009).
[12]M. F. Su, R. H. Olsson III, Z. C. Leseman, and I. El-Kady, Appl. Phys. Lett. **96**, 053111 (2010).
[13]C. Croënne, D. Manga, B. Morvan, A. Tinel, B. Dubus, J. O. Vasseur, and A.C Hladky-Hennion, Phys. Rev. B **83**, 054301 (2011).
[14]B. Morvan, A. Tinel, A.-C. Hladky-Hennion, J. Vasseur, and B. Dubus, Appl. Phys. Lett. **96**, 101905 (2010).
[15]A. Sukhovich, L. Jing, and J. H. Page, Phys. Rev. B **77**, 014301 (2008).
[16]A. Sukhovich, B. Merheb, K. Muralidharan, J. O. Vasseur, Y. Pennec, P. A. Deymier, and J. H. Page, Phys. Rev. Lett. **102**, 154301 (2009).
[17]I. Pérez-Arjona, V. J. Sánchez-Morcillo, J. Redondo, V. Espinosa, and K. Staliunas, Phys. Rev. B **75**, 014304 (2007).
[18]J. Bucay, E. Roussel, J. O. Vasseur, P. A. Deymier, A.-C. Hladky-Hennion, Y. Pennec, K. Muralidharan, B. Djafari-Rouhani, and B. Dubus, Phys. Rev. B **79**, 214305 (2009).
[19]C. Goffaux and J. P. Vigneron, Phys. Rev. B **64**, 075118 (2001).
[20]J. Baumgartl, M. Zvyagolskaya, and C. Bechinger, Phys. Rev. Lett. **99**, 205503 (2007).
[21]J.-Y. Yeh, Physica B **400**, 137 (2007).
[22]Z.-G. Huang and T.-T. Wu, IEEE Trans. Ultrason. Ferroelectr. Freq. Control **52**, 365 (2005).
[23]K. L. Jim, C. W. Leung, S. T. Lau, S. H. Choy, and H. L. W. Chan, Appl. Phys. Lett. **94**, 193501 (2009).
[24]K. Bertoldi and M. C. Boyce, Phys. Rev. B **77**, 052105 (2008).
[25]Z. Hou, F. Wu, and Y. Liu, Solid State Commun. **130**, 745 (2004).
[26]Y. Wang, F. Li, Y. Wang, K. Kishimoto, and W. Huang, Acta Mechanica Sinica **25**, 65 (2009).
[27]Y.-Z. Wang, F.-M. Li, W.-H. Huang, X. Jiang, Y.-S. Wang, and K. Kishimoto, Int. J. Solids Struct. **45**, 4203 (2008).
[28]Y.-Z. Wang, F.-M. Li, K. Kishimoto, Y.-S. Wang, and W.-H. Huang, Wave Motion **46**, 47 (2009).
[29]J.-F. Robillard, O. Bou Matar, J. O. Vasseur, P. A. Deymier, M. Stippinger, A.-C. Hladky-Hennion, Y. Pennec, and B. Djafari-Rouhani, Appl. Phys. Lett. **95**, 124104 (2009).
[30]J. R. Cullen, S. Rinaldi, and G. V. Blessing, J. Appl. Phys. **49**, 1960 (1978).
[31]T. Lapteva, O. Tarasenko, and S. Tarasenko, Phys. Solid State **49**, 1268 (2007).
[32]V. G. Bar'yakhar and E. A. Turov, *Spin Waves and Magnetic Excitations* 2, Vol. 7 (North-Holland, Amsterdam, 1988).
[33]Y. V. Gulyaev, I. E. Dikshtein, and V. G. Shavrov, Phys. Usp. **40**, 701 (1997).
[34]R. C. LeCraw and R. L. Comstock, *Physical Acoustics: Principles and Methods, Vol. III, Part B: Lattice Dynamics* (Academic, New York, 1965).
[35]S. Rinaldi and G. Turilli, Phys. Rev. B **31**, 3051 (1985).
[36]I. Mirsaev, Phys. Solid State **40**, 1884 (1998).
[37]M. Wilm, S. Ballandras, V. Laude, and T. Pastureaud, J. Acoust. Soc. Am. **112**, 943 (2002).
[38]T.-T. Wu, Z.-C. Hsu, and Z.-G. Huang, Phys. Rev. B **71**, 064303 (2005).
[39]P. Langlet, A.-C. Hladky-Hennion, and J. N. Decarpigny, J. Acoust. Soc. Am. **98**, 2792 (1995).
[40]A. G. Gurevich and G. A. Melkov, *Magnetization Oscillations and Waves* (CRC, Boca Raton, 1996).
[41]D. E. Eastman, Phys. Rev. **148**, 530 (1966).
[42]G. Simon, Z. Naturforsch **13A**, 84 (1958).
[43]J. Rouchy and E. du Tremolet de Lacheisserie, Z. Phys. B **36**, 67 (1979).
[44]R. L. Melcher, Phys. Rev. Lett. **25**, 1201 (1970).
[45]J. Smit and H. G. Beljers, Philips Res. Rep. **10**, 113 (1955).
[46]H. Suhl, Phys. Rev. **97**, 555 (1955).
[47]C. Kittel, Rev. Mod. Phys. **21**, 541 (1949).
[48]A. K. Ganguly, K. L. Davis, D. C. Webb, and C. Vittoria, J. Appl. Phys. **47**, 2696 (1976).
[49]A. K. Ganguly, K. L. Davis, and D. C. Webb, J. Appl. Phys. **49**, 759 (1978).
[50]V. Laude, Y. Achaoui, S. Benchabane, and A. Khelif, Phys. Rev. B **80**, 092301 (2009).
[51]V. Romero-Garcia, J. V. Sanchez-Perez, and L. M. Garcia-Raffi, J. Appl. Phys. **108**, 044907 (2010).
[52]B. A. Auld, *Acoustic Fields and Waves in Solids* (John Wiley & Sons, New York, 1973).
[53]V. A. Ignatchenko, H. Kronmüller, and M. Grönefeld, J. Magn. Magn. Mater. **89**, 229 (1990).
[54]E. Y. Tsymbal, Appl. Phys. Lett. **77**, 2740 (2000).